JOURNAL OF MATERIALS SCIENCE 23 (1988) 2622–2630

# Microstructure, chemistry, elastic properties and internal friction of Silceram glass–ceramics

S. CARTER, C. B. PONTON, R. D. RAWLINGS, P. S. ROGERS
*Department of Materials, Imperial College, London SW7 2BP, UK*

The temperature dependence of both Young's modulus ($E$) and internal friction ($Q^{-1}$) from room temperature to $\approx 700°$ C has been determined by Förster's forced-resonance method for three Silceram glass–ceramics, produced by the direct controlled cooling of glass melts in the quaternary system $CaO–MgO–Al_2O_3–SiO_2$. These results are correlated with microstructural and phase chemistry data as well as calculated viscosity against temperature data. In particular, the viscosity of the residual glass is shown to predominate over its volume fraction in determining the temperature dependence of $E$ and $Q^{-1}$ for a given Silceram. A simple model which enables the residual glass content of Silceram glass-ceramics to be estimated from a knowledge of the proportions of silicon, iron and magnesium in the corresponding glass melts is also proposed. Furthermore, the room-temperature bulk modulus ($K$) and Poisson's ratio of two Silceram glass–ceramics are calculated using experimental $E$ and shear modulus ($G$) values obtained using both Förster's method and another forced-vibration technique.

## 1. Introduction

Silceram glass–ceramics were developed as erosion- and abrasion-resistant materials. They are produced by direct controlled cooling of aluminosilicate melts made from either pure components or waste materials such as iron blast-furnace slag [1–4]. The principal oxide components in the melt are CaO, MgO, $Al_2O_3$, $SiO_2$, and iron oxides. Smaller quantities of chromium oxide are also present, and play a fundamental role in controlling the nucleation of crystals during the conversion from melt to glass–ceramic. This direct controlled cooling process is more economical [2–4] than the conventional glass–ceramic process, which involves two-stage re-heating of the parent glass to the optimum crystal nucleation and crystal growth temperatures.

Silcerams were initially designed for application at room temperature, and consequently attention has to date concentrated on the determination of their properties at this temperature. In particular, a study of the room-temperature mechanical properties, e.g. fracture toughness, fracture strength and hardness, has recently been completed [4]. During this study it became apparent that, in order to better understand the mechanical behaviour of the Silcerams, more detailed information on the microstructure and chemistry of the constituent phases would be required. Furthermore, it became obvious that there is considerable scope for diversifying the uses of Silcerams, and hence a knowledge of their mechanical behaviour at elevated temperatures would be desirable. For these reasons work on these topics was instigated.

This paper reports the results of an investigation, using electron microscopy, of the chemistry and microstructure of three Silcerams and correlates these results with the temperature dependence of both the Young's modulus and the internal friction. The internal friction of materials other than metallic and polymeric has not been widely studied, and to the authors' knowledge this is the first report on a glass–ceramic.

## 2. Experimental procedure

Three Silcerams, designated SCR25-76, SCR19-34 and SCF5, were used in the investigation. SCR25-76 and SCR19-34 were produced in 50 to 100 kg batches at a pilot plant, the former from iron blast-furnace slag, colliery shale and supplemental pure oxide components, and the latter from pure oxide and carbonate components [2–4]. SCF5 was made in the laboratory in 100 g melts using pure oxide and carbonate components [2–4]. In addition, a low-iron-content Silceram (SCR25-74) was deliberately produced at the pilot plant in order to ascertain the effect of iron content on the amount of residual glass. Furthermore, a poorly crystallized pilot-plant material (SCR19-13) was chosen for comparison with SCR25-76, SCR19-34 and SCF5 as regards the Young's modulus.

The microstructural investigation was conducted on specimens polished to a 1 $\mu$m surface finish, etched in 2% aqueous HF, vacuum-coated with gold and examined in a Jeol T200 scanning electron microscope (SEM). The proportions of the crystalline (pyroxene) and vitreous phases were determined by image analysis of the SEM micrographs using a Bausch and Lomb Omnicon TM3000 computer-based image analyser. Bulk chemical analyses were carried out on polished and carbon-coated specimens analysed using a Jeol JSM-35CF SEM equipped with energy-dispersive X-ray analysis (EDAX) facilities. The chemical compositions of the residual glass and the pyroxene crystalline phases were also determined using EDAX, but


0022–2461/88 $03.00 + .12 

in this case transmission electron microscopy (TEM) was employed. The thin samples required for TEM were prepared by ion-beam thinning and examined in a Jeol JEM-120CX scanning transmission electron microscope.

The elastic property and internal friction data were obtained using two forced-vibration techniques. Both techniques involved the forced vibration of straight bar specimens of uniform rectangular cross-section with the ends free, i.e. the so-called "free–free" vibration mode. The main experimental technique was used to determine (a) the Young's modulus and internal friction at both room and elevated temperatures, and (b) the room-temperature shear modulus. The subsidiary method was only employed for room-temperature Young's and shear-modulus measurements. The experimental arrangement for the main method was due to Förster [5] and involved horizontally suspending the specimen on two flexible fibre or wire supports from the exciting and detecting transducers. An elliptical focusing radiation furnace, based on the design of Lytton *et al.* [6], was used to obtain the elevated temperatures. The apparatus could be evacuated in order to minimize oxidation of the polished surfaces of the furnace and to reduce air-damping of the specimen vibrations. The subsidiary technique involved clamping the specimen at the nodes using two pairs of opposing knife-edges, and exciting and detecting resonance using rigid driver and pick-up probes in direct contact with the specimen surface. This apparatus was not designed for work under vacuum nor for work at elevated temperatures.

The rectangular cross-section specimens used to determine the Young's modulus, $E$, had nominal dimensions of 80 mm × 12 mm × 3 mm and were hung from loops in the flexible fibre or wire supports. The equation used to calculate $E$ from the fundamental flexural resonant frequency, $f_F$, was [7]

$$E = 0.94642 \left(\frac{L}{t}\right)^3 \left(\frac{M}{b}\right) f_F^2 A \quad (1)$$

where $L$, $b$, $t$ and $M$ are the specimen length, width, thickness and mass, respectively, and $A$ is a correction factor which is a function of Poisson's ratio, $v$, and the thickness-to-length ratio, $t/l$. The Young's modulus was measured as a function of the position of the supports in air and under vacuum at room temperature, and as a function of temperature under vacuum.

Similar rectangular cross-section specimens were used for the shear-modulus measurements, but with the thickness reduced to 1.4 mm. When using the main technique, torsional vibrations were induced by gluing the support fibres to each thin side of the specimen at the flexural nodes such that they were diagonally opposed. In contrast, the specimen was clamped at the torsional node when employing the subsidiary method. The shear modulus, $G_M$, which was measured only at room temperature, was calculated from the fundamental torsional resonant frequency, $f_T$, using the equation [8, 9]

$$G_M = \frac{G_E}{1 + C} \quad (2)$$

where $C$ is an empirical correction factor dependent on the width-to-thickness ratio, $b/t$, and $G_E$ is the experimental shear modulus given by the theoretical approximation [10]

$$G_E = SM f_T^2 \quad (3)$$

where $M$ is the specimen mass and $S$ a shape factor.

The internal friction, $Q^{-1}$, was calculated from the resonance peak obtained in the fundamental flexural vibration mode using [11, 12]

$$Q^{-1} \equiv \frac{f_U - f_L}{3^{1/2} f_F} \quad (4)$$

where $f_U$ and $f_L$ are the driven frequencies above and below $f_F$, respectively, at which the vibrational amplitude is half the maximum value.

## 3. Experimental results

### 3.1. Composition, microstructure and viscosity calculations

The microstructures of the Silcerams are shown in Figs 1 to 6. The pyroxene phase in the laboratory material (SCF5) has a well-developed dendritic structure (Fig. 1). The backbone of the dendrites reached a length of 30 $\mu$m, whereas the dendrite arm-length and arm-width did not exceed 10 $\mu$m and $\approx 1$ $\mu$m, respectively. Neighbouring dendrites were intermeshed, resulting in an almost continuous pyroxene network which extended throughout the sample. The SCF5 material was the most crystalline with a residual glass content of only 18 ± 5% by volume. The pyroxene crystals in the pure oxide pilot-plant Silceram (SCR19-34) were much finer and less dendritic (Fig. 2), and their more equiaxed shape, coupled with the greater residual glass content of SCR19-34 (42 ± 2 vol %), meant that the pyroxene crystals were discrete rather than intermeshed. The microstructure of the iron blast-furnace slag based material (SCR25-76) was the least dendritic (Fig. 3), and in places tended towards euhedral morphology. The pyroxene phase was homogeneously distributed throughout the glass matrix and had a crystal size of 3 to 8 $\mu$m. The residual glass content was 29 ± 3 vol %. The microstructure of SCR25-74 (Fig. 6) was very similar to that of SCR25-76 except for a slightly larger grain size of $\approx 10$ $\mu$m and a glass content of 37 ± 3 vol %. The poorly crystallized SCR19-13 material (Figs 4 and 5) had a glass content of 70 ± 8 vol %.

The results of the chemical analyses of the bulk materials are given in Table I, while the chemical analysis results for the pyroxene and residual glass phases in SCR25-74, SCR25-76, SCR19-34 and SCF5 are presented in Table II. The bulk composition data show that the SCR25 samples are less siliceous and contain more CaO and slightly more $Al_2O_3$ than SCR19-34, whilst the MgO content remains approximately constant. SCR25-74 is significantly lower in iron than SCR25-76 and SCR19-34. The laboratory material SCF5 is very high in both $SiO_2$ and MgO compared to the outer samples; however, its $Fe_2O_3$ and CaO contents are relatively low. Comparison of the compositions of the pyroxene and residual glass phases indicates that the residual glass was higher in $SiO_2$ and $Al_2O_3$, while almost all the MgO and $Fe_2O_3$

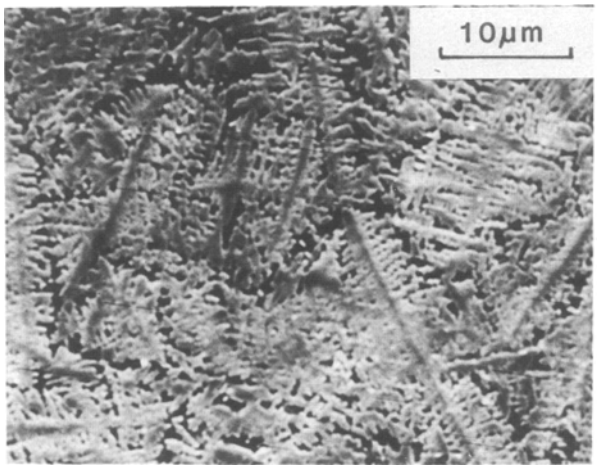


*Figure 1* SEM micrograph of SCF5 microstructure.

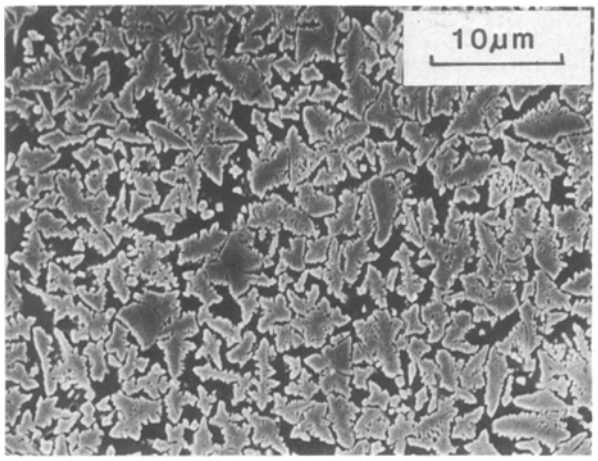


*Figure 2* SEM micrograph of SCR19-34 microstructure.

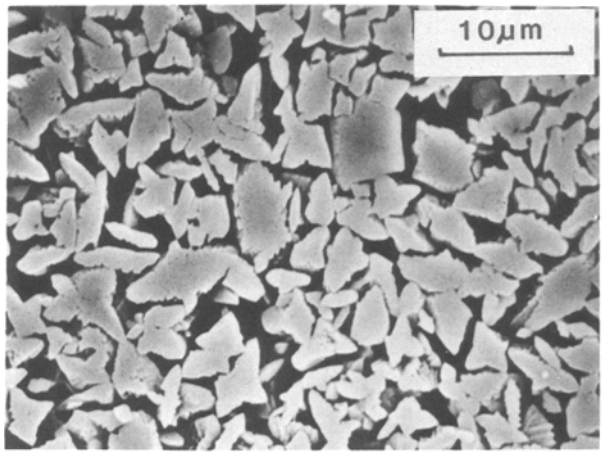


*Figure 3* SEM micrograph of SCR25-76 microstructure.

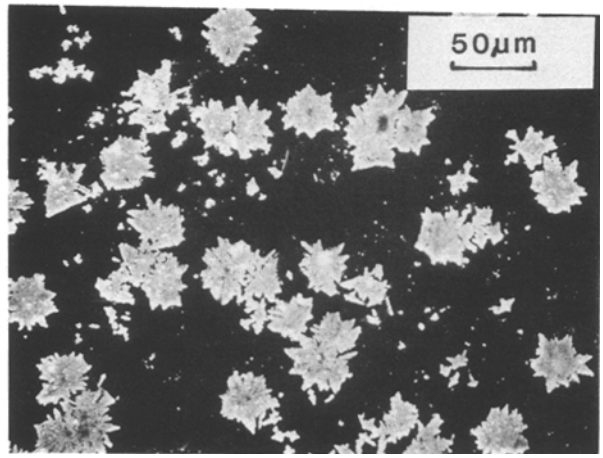


*Figure 4* SEM micrograph of SCR19-13 microstructure.

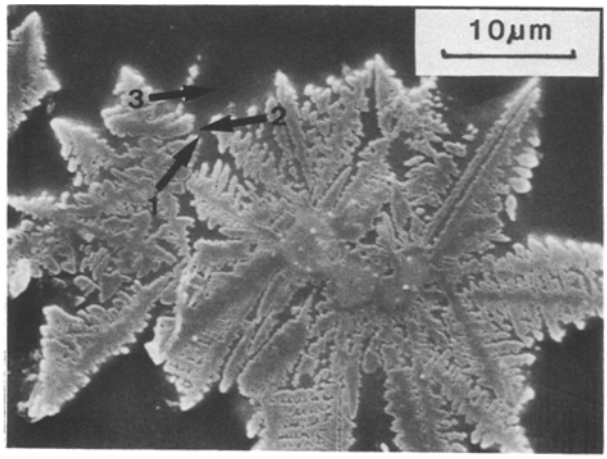


*Figure 5* SEM micrograph of SCR19-13 showing the three areas (arrowed) of residual glass representative of the areas chemically analysed by EDAX of thin-foil samples using TEM.

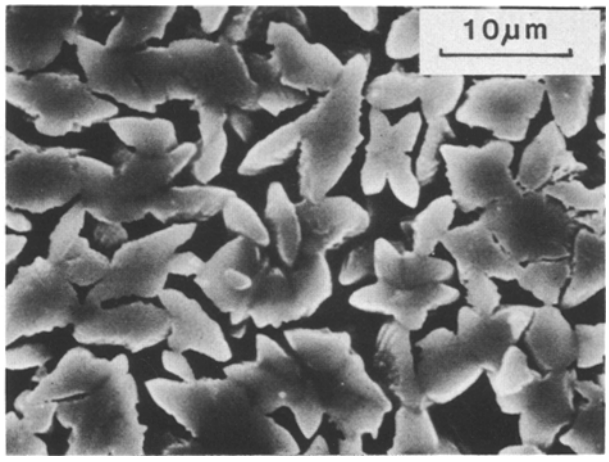


*Figure 6* SEM micrograph of SCR25-74 microstructure.

was contained in the pyroxene phase. The CaO content of the residual glass was either similar to that of the pyroxene phase as in the SCR25 samples, or less than that of the pyroxene phase as in the SCR19-34 and SCF5 samples. The pyroxene and residual glass compositions of SCR19-13 were also analysed; the glass was analysed as a function of distance from the pyroxene phase, i.e. adjacent to the crystal–glass interface (e.g. Area 1 in Fig. 5), further away from the interface (e.g. Area 2 in Fig. 5), and far away from any interface (e.g. Area 3 in Fig. 5). The results are given in Table III.

The method of Urbain *et al.* [13] was used to calculate the viscosities of both the melts of the bulk compositions and the corresponding residual glasses. Both the changes in viscosity of SCR25-74, SCR25-76, SCR19-34 and SCF5 during crystallization at 950° C and the temperature ranges of the dilatometric

TABLE I Chemical compositions of the Silcerams

| Oxide | Sample | | | |
|---|---|---|---|---|
| | SCF5 | SCR19-34 | SCR25-76 | SCR25-74 |
| Normalized content (wt %) | | | | |
| $SiO_2$ | 56.4 | 52.8 | 48.3 | 48.8 |
| $TiO_2$ | 0.2 | 0.3 | 0.6 | 0.5 |
| $Al_2O_3$ | 13.2 | 12.5 | 13.3 | 13.5 |
| $Cr_2O_3$ | 0.7 | 0.8 | 0.8 | 1.0 |
| $Fe_2O_3$ | 2.8 | 4.6 | 4.0 | 2.3 |
| MnO | – | 0.1 | 0.4 | 0.5 |
| MgO | 9.7 | 5.9 | 5.7 | 5.9 |
| CaO | 16.3 | 20.1 | 24.7 | 25.3 |
| $Na_2O$ | 0.4 | 2.8 | 1.2 | 1.3 |
| $K_2O$ | 0.4 | 0.1 | 1.1 | 1.0 |
| Content of mono-cationic oxide (mol %) | | | | |
| $SiO_2$ | 52.3 | 49.0 | 45.1 | 45.3 |
| $TiO_2$ | 0.1 | 0.2 | 0.4 | 0.3 |
| $AlO_{1.5}$ | 14.4 | 13.7 | 14.6 | 14.8 |
| $CrO_{1.5}$ | 0.5 | 0.6 | 0.6 | 0.7 |
| $FeO_{1.5}$ | 1.9 | 3.2 | 2.8 | 1.6 |
| MnO | – | 0.1 | 0.3 | 0.4 |
| MgO | 13.4 | 8.2 | 7.9 | 8.2 |
| CaO | 16.1 | 20.0 | 24.7 | 25.2 |
| $NaO_{0.5}$ | 0.7 | 5.0 | 2.2 | 2.3 |
| $KO_{0.5}$ | 0.5 | 0.1 | 1.3 | 1.2 |

softening points of the residual glasses were estimated from the corresponding calculated viscosity against temperature data (Table IV). The dilatometric softening point ($T_D$) is the temperature at which the viscosity is in the range $10^{10}$ to $10^{11}$ Pa sec and the thermal expansion is counteracted by viscous flow when the thermal expansion is measured by dilatometry (see [14] for example).

## 3.2. Mechanical properties

The shear-modulus values obtained in air by the horizontal clamping method and under vacuum by the suspension technique were in good agreement (Table V). As regards the Young's modulus, it was found that the suspension position, atmosphere (Fig. 7) and exciting amplitude had a negligible effect on the value obtained by the suspension technique; consequently the mean $E$ values from all the data regardless of suspension position and atmosphere are presented in Table V, together with the mean $E$ values determined by the horizontal clamping method. The mean $E$ values from the clamping technique are in reasonable agreement with those from the suspension method for SCR25-76 and SCF5, but there is a discrepancy of some 7% in the case of SCR19-34. The Poisson's ratio

TABLE II Composition (wt %) of pyroxene crystals (PX) and residual glass (RG) in the Silcerams

| Oxide | SCF5 | | SCR19-34 | | SCR25-76 | | SCR25-74 | |
|---|---|---|---|---|---|---|---|---|
| | PX | RG | PX | RG | PX | RG | PX | RG |
| $SiO_2$ | 52.2 | 66.1 | 47.0 | 58.0 | 45.6 | 53.2 | 47.3 | 53.4 |
| $TiO_2$ | 0.4 | 0.4 | 0.2 | 1.1 | 1.0 | 0.5 | 0.8 | 0.5 |
| $Al_2O_3$ | 9.6 | 18.0 | 8.3 | 15.1 | 10.7 | 16.6 | 10.7 | 14.9 |
| $Cr_2O_3$ | 0.7 | 1.0 | 1.0 | 0.2 | 1.7 | 0.1 | 1.3 | 0.3 |
| $Fe_2O_3$ | 4.0 | 1.1 | 8.7 | 2.5 | 6.3 | 1.1 | 4.3 | 0.9 |
| MnO | 0.1 | 0.1 | 0.1 | 0.1 | 0.7 | 0.3 | 0.5 | 0.6 |
| MgO | 12.9 | 1.3 | 10.0 | 1.3 | 7.7 | 0.1 | 9.2 | 0.4 |
| CaO | 19.3 | 10.0 | 24.4 | 19.3 | 25.4 | 25.5 | 25.4 | 26.3 |
| $Na_2O$ | 0.5 | 1.1 | 0.4 | 2.0 | 0.7 | 0.3 | 0.3 | 0.6 |
| $K_2O$ | 0.2 | 0.9 | Tr. | 0.3 | 0.3 | 2.2 | 0.2 | 2.1 |

TABLE III Composition (wt %) of the crystalline phase of SCR19-13 and its residual glass as a function of distance from the glass–crystal interface

| Oxide | Crystal | Residual glass* | | |
|---|---|---|---|---|
| | | 1 | 2 | 3 |
| $SiO_2$ | 47.4 | 61.9 | 55.6 | 52.1 |
| $TiO_2$ | 0.1 | 1.2 | 0.8 | 0.9 |
| $Al_2O_3$ | 7.7 | 15.8 | 15.2 | 12.3 |
| $Cr_2O_3$ | 0.7 | 0.6 | 0.6 | 0.5 |
| $Fe_2O_3$ | 8.1 | 1.7 | 4.1 | 4.0 |
| MnO | 0.0 | 0.0 | 0.0 | 0.2 |
| MgO | 10.2 | 1.7 | 4.1 | 4.0 |
| CaO | 25.8 | 12.8 | 15.7 | 25.0 |
| $Na_2O$ | 0.0 | 3.1 | 3.8 | 0.9 |
| $K_2O$ | 0.1 | 1.2 | 0.2 | 0.1 |

*(1) Residual glass adjacent to the interface from an area such as Area 1 in Fig. 5; (2) residual glass near the interface (but further away than Case 1) from an area such as Area 2 in Fig. 5; (3) residual glass far from the interface from an area such as Area 3 in Fig. 5.

($\nu$) values and the previously presented $E$ values for SCR25-76 and SCR19-34 were calculated iteratively on a computer using the respective shear moduli and Equations 1 and 5:

$$\nu = \frac{E}{2G} - 1 \tag{5}$$

The Poisson's ratio so obtained, and values for the bulk modulus calculated assuming linear elastic and elastically isotropic behaviour [15], are also given in Table V.

The internal friction was not affected by a factor-of-five change in the exciting amplitude. In contrast to $E$, however, $Q^{-1}$ varied markedly with suspension position and generally the values under vacuum were slightly lower than those in air (Fig. 8). The position dependence of $Q^{-1}$ was in accordance with the theory proposed by Wachtman and Tefft [16] and is demonstrated by the good fit of the theoretical curve for SCR25-76 in air to the experimental data (Fig. 9).

The Young's modulus at a test temperature $T$ above room temperature was corrected for the change in specimen dimensions due to thermal expansion by use of the equation [17]

$$M = M_R \left(\frac{f}{f_R}\right)^2 \frac{1}{1 + \alpha\Delta T} \tag{6}$$

where $M$ is the elastic modulus at temperature $T$, $M_R$ the elastic modulus at room temperature, $f$ the resonant frequency at $T$, $f_R$ the resonant frequency at room temperature, $\alpha$ the average linear thermal expansivity of the material from room temperature to $T$, and $\Delta T$ the differential temperature. As the correction for thermal expansion is not very sensitive to the value for $\alpha$, the $\alpha$ value for SCF5 between room temperature and 800° C of $7.5 \times 10^{-6}\,K^{-1}$ [2] was used for all the Silcerams. The Young's modulus was determined as a function of temperature with the specimen suspended at 6, 8, and 10 mm outside the nodes and the results normalized to the room-temperature value at the commencement of a run. This procedure produced a single curve for the temperature dependence of a given Silceram as shown in Fig. 10. The Young's modulus of each of the Silcerams is a linear function of temperature up to a temperature characteristic of a particular Silceram, at which point $E$ begins to decrease non-

TABLE IV Calculated viscosity ($\eta$) at 950° C and the dilatometric softening point ($T_D$) range of the residual glass of Silceram glass–ceramics

| Property | Sample | | | |
|---|---|---|---|---|
| | SCF5 | SCR19-34 | SCR25-76 | SCR25-74 |
| log (bulk $\eta$)* | 3.0 | 2.8 | 2.5 | 2.6 |
| log (resid. glass $\eta$)* | 6.3 | 4.4 | 3.9 | 3.5 |
| $\Delta$ log $\eta$* | 3.3 | 1.6 | 1.4 | 0.9 |
| $T_D$ (° C)† | 630 to 680 | 480 to 520 | 440 to 480 | 410 to 450 |

*log $\eta$ at 950° C where $\eta$ is the viscosity in Pa sec;
†$\eta = 10^{10}$ to $10^{11}$ Pa sec.

TABLE V Room-temperature elastic constants for Silceram glass–ceramics

| Sample | $G$(GPa)* | | $E$(Gpa)* | | $K$(GPa) | $\nu$ |
|---|---|---|---|---|---|---|
| | S | C | S | C | | |
| SCR25-76 | 49.7 | 49.3 | 121.7 ± 1.5 | 118 ± 8 | 73 | 0.23 |
| SCR19-34 | 47.7 | 47.8 | 115.0 ± 0.2 | 107 ± 4 | 65 | 0.21 |
| SCF5 | – | – | 120.6 ± 0.9† | 121 ± 7† | | |
| SCR19-13 | – | – | 100.6† | | | |

*S = suspension technique value, C = horizontal clamping technique value.
†Calculated assuming $\nu = 0.25$.

linearly. Table VI gives the parameters of the linear equation

$$E = a + bT \quad (7)$$

and the characteristic temperature $T_C$ as determined by computer analysis.

The internal friction could not be measured to such high temperatures as the Young's modulus because either (i) although the resonant frequency could be detected, the amplitude at resonance was barely above the background amplitude and consequently the width of the resonance peak at half maximum amplitude could not be measured, or (ii) the resonance peak was asymmetrical, presumably due to a spurious resonance of the system. Even though $Q^{-1}$ varied with suspension position, normalizing to the appropriate room-temperature value yielded a single temperature-dependent curve for each Silceram, albeit with a greater scatter than the Young's modulus data. From the normalized curves of Fig. 10 it can be seen that $Q^{-1}$ at first increases gradually in a linear manner with temperature and then begins to rise more rapidly. The temperature at which $Q^{-1}$ begins to rise rapidly ($T_Q$) increases in the order SCR25-76, SCR19-34, SCF5, which is the same sequence shown by the characteristic temperature of the Young's modulus curves. For a given Silceram, however, $T_C$ is much higher than $T_Q$ (see Table VI).

## 4. Discussion

### 4.1. Residual glass

As the residual glass plays an important role in determining the properties of glass–ceramics, it would be useful to be able to estimate the residual glass content

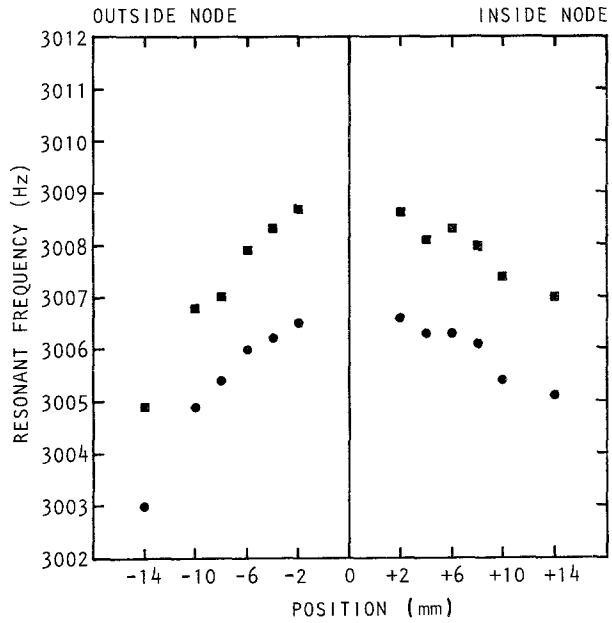


*Figure 7* Graph showing that the typical dependence of the fundamental flexural resonant frequency on the suspension position (●) in air and (■) under vacuum is small, and so will have a negligible effect on the calculated value for Young's modulus.

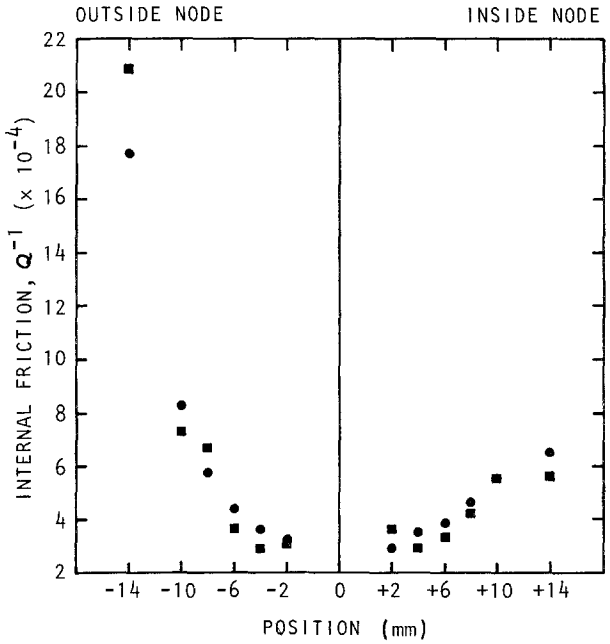


*Figure 8* Typical plot of internal friction as a function of suspension position (●) in air and (■) under vacuum, showing that it is generally lower under vacuum.

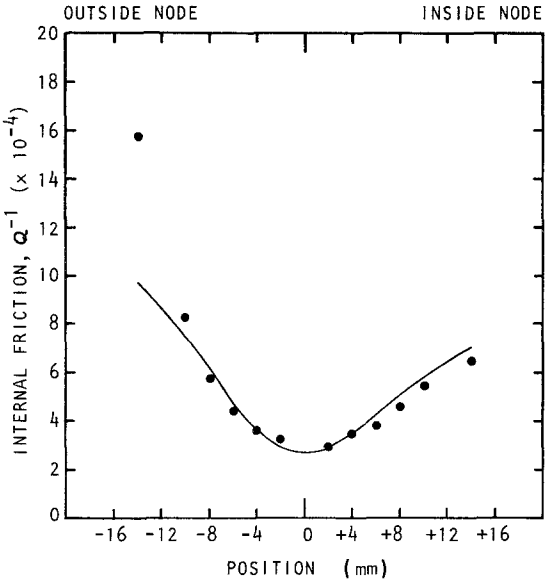


*Figure 9* Internal friction data for a specimen of SCR25-76 in air superposed on the theoretical curve for the suspension position dependence proposed by Wachtman and Tefft [16].

from the composition of the melt. A simple analysis is proposed whereby the residual glass content in the Silcerams under investigation may be estimated from the proportions of silicon, iron and magnesium in the melt.

The bulk compositions of the melt are very close to pyroxene compositions and, in theory, nearly all the material could be used to form pyroxenes. In practice, however, varying amounts of residual glass were formed in the four materials SCF5, SCR25-76, SCR25-74 and SCR19-34, all of which had been produced under similar melting and heat-treatment schedules. The composition of pyroxenes can be expressed in the following form (see [18] for example):

$$Ca_{1-p}(Mg, Fe)_{1+p}(Si, Al)_2O_6$$

where a wide range of ionic substitution is possible

TABLE VI The parameters in the equation $E = a + bT$, the characteristic temperature $T_C$ at which the linear dependence of $E$ breaks down, and the onset temperature $T_Q$ at which the internal friction $Q^{-1}$ begins increasing in a strongly non-linear manner

| Sample | $a$ (Pa) | $b$ (Pa (°C)$^{-1}$) | $T_C$ (°C) | $T_Q$ (°C) |
|---|---|---|---|---|
| SCR25-76 | $122.8 \times 10^9$ | $-1.90 \times 10^7$ | 436 | ≈250 |
| SCR19-34 | $114.7 \times 10^9$ | $-1.53 \times 10^7$ | 551 | ≈430 |
| SCF5 | $121.3 \times 10^9$ | $-1.06 \times 10^7$ | 626 | ≈550 |

between the following end-members:

| | |
|---|---|
| $CaMgSi_2O_6$ | diopside |
| $CaFeSi_2O_6$ | hedenbergite |
| $MgSiO_3$ | enstatite |
| $FeSiO_3$ | ferrosilite |

In these pyroxenes, calcium can be further substituted by sodium, while aluminium can substitute for up to 10 mol % Si in the $SiO_4$ tetrahedra as well as entering the magnesium and iron positions to form an aluminous component, known as tschermakite, which has the formula $CaAl_2SiO_6$. The partitioning of aluminium between the melt and the pyroxene as it crystallizes is complex and is affected by factors such as temperature, pressure, and variations in the composition of the melt.

Previous X-ray studies [4] showed that the pyroxenes formed in these materials are close to diopside. Chemical analyses confirmed this and also indicated that between 6 and 12 mol % of tschermakite was present in the diopside solid solution. In addition, small amounts of enstatite were observed in SCF5. Analyses of the residual glasses of the materials indicated that only very small amounts of magnesium and iron were present in the glass; nearly all the magnesium and iron was present in the pyroxenes (see Table II).

The proposed analysis relates the residual glass content to the excess of silica in the melt over that

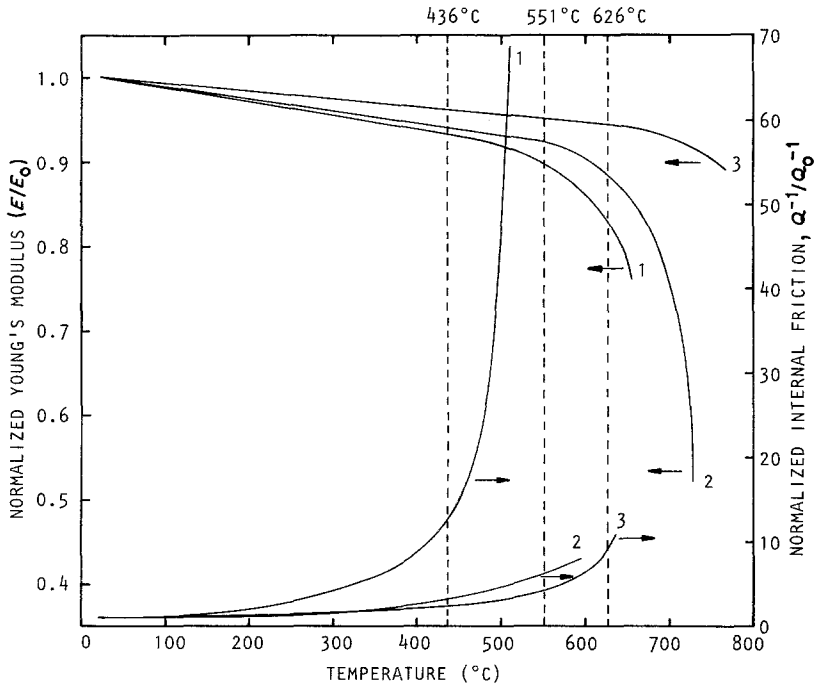


*Figure 10* Graph of the normalized Young's modulus ($E/E_0$) and normalized internal friction ($Q^{-1}/Q_0^{-1}$) of (1) SCR25-76, (2) SCR19-34 and (3) SCF5 as a function of temperature.

required for pyroxene formation. The following assumptions were made:

(a) the pyroxene compositions were near the diopside–hedenbergite solid solution (i.e. the enstatite and/or ferrosilite content must be small);

(b) the partitioning of aluminium between the melt and the crystalline phase is broadly similar, and

(c) all the samples were produced under the same melting and heat-treatment conditions.

These assumptions are reasonable in the case of the present materials which covered a limited range of melt compositions, with nominally the same amount of $Al_2O_3$ ($\approx$ 12 to 13 wt %), and had similar thermal histories. In these circumstances, as nearly all the magnesium and iron was present in the pyroxenes, the molar sum of (Mg + Fe) in the bulk analysis can be used to estimate the number of moles of silica required for pyroxene formation. The nature of the pyroxene formula is such that

$$\sum \text{moles(Ca + Mg + Fe)} = \text{moles(Si)} \quad (8)$$

and that

$$\text{moles(Ca)} \leqslant \sum \text{moles(Mg + Fe)} \quad (9)$$

Since the pyroxenes in the present study are basically of diopsidic composition, it is assumed that

$$\text{moles(Ca)} = \sum \text{moles(Mg + Fe)} \quad (10)$$

and that the number of moles of silicon, and hence $SiO_2$, needed for pyroxene formation can be estimated as

$$\text{moles(Si)} = 2 \sum \text{moles(Mg + Fe)} \quad (11)$$

The remaining silica in the melt composition is considered to be the excess silica forming the residual glass. As shown in Fig. 11 and Table VII, the excess $SiO_2$ correlates well with the volume fraction of residual glass estimated by the image analyses despite the fact that the effect of $Al_2O_3$ has not been taken into account. However, further data are needed to confirm whether or not Fig. 11 could be used to estimate the amount of residual glass directly from the melt compositions over a wider range of compositions and production procedures.

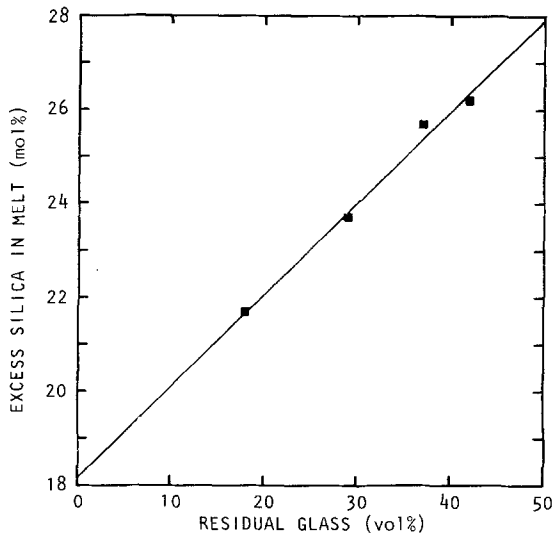


*Figure 11* Graph illustrating the linear relationship between the excess silica in a Silceram melt and the volume fraction of residual glass.

TABLE VII Volume fraction of residual glass and excess silica in Silceram glass-ceramics

| Property | Sample | | | |
|---|---|---|---|---|
| | SCF5 | SCR19-34 | SCR25-76 | SCR25-74 |
| Residual glass (vol %) | 18 ± 5 | 42 ± 2 | 29 ± 3 | 37 ± 3 |
| Excess $SiO_2$ (mol %) | 21.7 | 26.2 | 23.7 | 25.7 |

## 4.2. Crystal morphology

The difference in morphology of the pyroxenes is attributed to the concentration and viscosity gradients established within the material during crystallization. As pyroxene crystallizes, the areas adjacent to the crystal–glass interface become depleted in magnesium, iron and, in some cases, also in calcium, e.g. SCF5 and SCR19-34. This can be seen from the analyses of the glass in the poorly crystallized sample SCR19-13 (see Table III); the areas adjacent to the crystals are more siliceous than those further away. The relative scarcity of modifying elements results in the siliceous regions near the interface being of higher viscosity. Such concentration and viscosity gradients destabilize the interface. According to Kirkpatrick [19] and Weston and Rogers [20] an unstable interface is formed when the crystal can grow faster further away from the interface than near it. It follows that any small perturbation on the growth front can quickly grow away from the rest of the crystal. Hence stable interfaces are characterized by flat planar surfaces, and as the degree of instability increases, the stable width of a flat crystal–melt interface surface decreases; i.e. with progressively increasing interface instability the morphology changes from euhedral to skeletal grains, then to dendritic grains, and finally to spherulitic grains.

This was confirmed by Kirkpatrick [19] and Donaldson *et al.* [21] who described the dependence of crystal morphology on the degree of undercooling and on the rate of cooling, respectively. The degree of instability is given by the ratio of diffusion rate to growth rate; the lower the ratio, the greater the interface instability. The ratio decreases with increasing undercooling or increasing cooling rate. This is because diffusion rates decrease with decreasing temperature and increasing viscosity, whereas the corresponding crystal growth rate increases initially and later decreases, although less rapidly than the diffusion rate. It has been found that at small undercoolings [19] (i.e. temperatures just below the liquidus temperature) or at slow cooling rates [21] euhedral tabular crystals were formed. As the degree of undercooling increased or as the cooling rate increased, the crystals became skeletal in form. Dendrital morphology was attained at even higher undercoolings or cooling rates, and eventually spherulitic crystallization occurred at very high undercoolings or cooling rates.

These same concepts may be applied to the crystal

growth which occurs during the isothermal heat-treatment of Silcerams. During isothermal heat-treatment the diffusion rate near the crystal–glass interface would be reduced due to the higher viscosity of the siliceous layer. Therefore the crystal can grow faster further away from the interface where also the concentration of modifying elements (magnesium, iron, calcium) necessary for the crystallization of the pyroxene is higher. Hence the greater the concentration and viscosity gradients, the more unstable is the interface and the more dendritic are the crystals.

The pyroxene morphologies in the Silcerams are consistent with this supposition. The greatest concentration and viscosity gradients would have been established in samples with the largest difference between the bulk composition and the residual glass composition. Thus the smallest concentration and viscosity gradients would be achieved in SCR25-76 and SCR25-74, and consequently their microstructures consisted of subhedral grains, tending in parts towards euhedral morphology, with relatively large, flat crystal–glass interfaces. The greater concentration and viscosity gradients in SCR19-34 resulted in a greater degree of dendritic growth, whilst the highly dendritic microstructure of SCF5 is associated with the greatest concentration and viscosity gradients.

### 4.3. Mechanical properties

The room-temperature elastic properties of the Silceram glass–ceramics compared very well with those of other glass–ceramics, as shown in Table VIII, especially in view of the relatively high volume fractions of residual glass in SCR19-34 and SCR25-76. The temperature dependence of the Young's modulus of the Silceram glass–ceramics will be discussed in conjunction with the temperature dependence of the internal friction. The viscosities of the residual glasses of the Silcerams SCF5, SCR19-34 and SCR25-76 decrease in the order SCF5 > SCR19-34 > SCR25-76 and the mid-band dilatometric softening temperatures are 655, 500 and 460° C, respectively (see Table IV). This sequence is also followed by the characteristic temperature ($T_C$) which indicates the empirical upper limit of the linear temperature dependence of the Young's moduli of the Silcerams (see Table VI). Furthermore, the $T_C$ values are all within 50° C of the corresponding mid-band dilatometric softening temperatures.

The volume fraction of residual glass decreases in the order SCR19.13 > SCR19.34 > SCR25.76 > SCF5; this order correlates inversely with the room-temperature elastic constants but bears no relationship to the observed $T_C$ and $T_Q$ values. Thus the viscosity of the residual glass appears to dominate the effect of the volume fraction of residual glass on the temperature dependence of the Young's modulus. This is illustrated by the fact that although the room-temperature Young's modulus of SCR19-34 is lower than that of SCR25-76, the relative decrease in Young's modulus with increasing temperature is less and the linear dependence maintained to a higher temperature (110° C higher) than that of SCR25-76 (see Table VI). Note that the lower volume fraction of higher-viscosity residual glass in SCF5 endowed it with the best overall mechanical behaviour, i.e. room-temperature and refractory behaviour.

TABLE VIII Room-temperature elastic properties of Silcerams in comparison with other glass–ceramics*

| Glass–ceramic | $E$ (GPa) | $G$ (GPa) | $K$ (GPa) | $\nu$ |
|---|---|---|---|---|
| SCR25-76 | 122 | 50 | 73† | 0.23 |
| SCR19-34 | 115 | 48 | 65† | 0.21 |
| SCF5 | 121 | – | – | – |
| SCR19-13 | 101 | – | – | – |
| Pyroceram C9606 (Corning)‡ | 120 | – | – | 0.24 |
| Pyroceram C9608 (Corning)‡ | 88 | – | – | 0.25 |
| EE 1087 (GEC Ceramics Ltd)‡ | 92 | 37 | – | 0.245 |
| Zerodur (Schott)‡ | 84 | – | – | – |

*All comparative data are typical room-temperature values after Morrell [25].
†Calculated values.
‡Commercial trade names.

An early study by Wachtman and Lam [22] of the temperature dependence of the Young's modulus and internal friction of single and polycrystalline alumina, as well as other refractory ceramics, using Förster's technique found that within experimental limits, the internal friction of single-crystal alumina (i.e. sapphire (99.9% $Al_2O_3$) and ruby (99.25% $Al_2O_3$ + 0.75% $Cr_2O_3$) was essentially independent of temperature up to the highest temperature of measurement (1400 and 1700° C for sapphire and ruby, respectively). It was also found that the internal friction of polycrystalline alumina varied little between room temperature and 800° C, but increased rapidly above 800° C. The scatter in the data from successive tests was such that no curve of internal friction against temperature above 800° C could be plotted; the drastic reduction in the vibrational amplitude at resonance due to the increase in internal friction established the maximum temperature at which the resonant frequency, and hence the internal friction, could be reliably measured. Furthermore, Wachtman and Lam found that the rapid increase in internal friction at high temperatures was accompanied by a rapid non-linear decrease in Young's modulus for all the polycrystal ceramics studied; this behaviour was attributed to grain boundary sliding.

The temperature dependence of the Young's modulus and internal friction of polycrystalline yttrium oxide ($Y_2O_3$) from room temperature to 1658° C has been investigated by Marlowe and Wilder [23]. They found that the Young's modulus decreased rapidly, in a non-linear manner, with increasing temperature between 1350 and 1658° C, and was accompanied by a rapid increase in the internal friction. Furthermore, the internal friction did not decrease with increasing temperature to its former level; Marlowe and Wilder concluded that the temperature of the peak of the internal friction curve was probably not reached. This rapid decrease in $E$ and the concomitant rapid increase in internal friction at high temperatures was analogous to the general behaviour of the polycrystalline ceramics investigated by Wachtman and Lam [22], e.g. for alumina between 800 and 1200° C.

A recent study of the temperature dependence (to 650 or 800° C) of the Young's modulus and internal

friction of partially stabilized zirconia (3 mol % $Y_2O_3$ + $ZrO_2$), alumina, and silicon nitride [24] found that the internal friction of alumina was relatively constant up to the maximum test temperature of 650° C (supporting the results of Wachtman and Lam [22]), while that of silicon nitride increased between 750 and 800° C (the maximum test temperature) which was attributed to the softening of the vitreous grain boundary phase deriving from the additive (3 wt % MgO) used to promote pressureless sintering. The internal friction of the partially stabilized zirconia increased rapidly with temperature up to a maximum at 200° C and then decreased rapidly with increasing temperature up to 400° C, and was thereafter similar to the room temperature value. The peak in the internal friction at 200° C coincided with an inflection in the Young's modulus against temperature curve, which decreased non-linearly with temperature up to 400° C but thereafter decreased linearly up to 650° C. The internal friction peak was suggested as possibly being due to twin motion in monoclinic $ZrO_2$ or the bowing of dislocations.

In summary, the bulk of the literature data on the temperature dependence (above room temperature) of the internal friction and Young's modulus in various conventional polycrystalline ceramics (i.e. not yttria-stabilized zirconia) such as alumina, magnesia, silicon nitride and so on, indicate that the rapid, non-linear decrease in the Young's modulus which usually occurs at elevated temperatures is accompanied by a rapid increase in the internal friction, which has been generally attributed to grain boundary sliding. The reasons for attributing this behaviour to a grain boundary energy-dissipation mechanism are as follows:

(a) Wachtman and Lam [22] found that no change occurred in the temperature dependence of the Young's modulus of single-crystal alumina (from linear to non-linear) at $\approx$ 950° C as observed for polycrystalline alumina.

(b) Furthermore, the internal friction of single-crystal alumina was essentially independent of temperature both above and below 950° C, unlike that of polycrystalline alumina which increased extremely rapidly with temperature above 950° C.

In the Silceram materials SCF5, SCR19-34 and SCR25-76, the rapid non-linear decrease in the Young's modulus and the rapid increase in the internal friction (starting at a lower temperature, $T_Q$, than the characteristic temperature, $T_C$, at which the temperature dependence of the Young's modulus became non-linear; see Table VI) correlated reasonably well with the estimates of the dilatometric softening-temperature bands of the intergranular residual glass. At elevated temperatures, the residual glass is anelastically strained under the action of the imposed periodic flexural stress due to its lower viscosity, and hence its tendency to flow. This time-dependent strain response is manifested as markedly higher internal friction at elevated temperatures, particularly at temperatures above the dilatometric softening point of the residual glass.

## Acknowledgements

The authors gratefully acknowledge the financial support of the SERC and the provision of laboratory facilities by Professor D. W. Pashley FRS. We thank Dr J. F. Bell and Miss M. Campbell for their help with the viscosity computations, and for producing the pilot-plant Silcerams and the laboratory Silceram, respectively.

## References

1. P. S. ROGERS, J. WILLIAMSON and P. E. JOHNSON, UK Patent 1 462 035 (1974) and US Patent 3 901 716 (1975).
2. P. S. ROGERS, J. WILLIAMSON, J. F. BELL and M. CAMPBELL, in Proceedings of Contractors' Meetings, Brussels, May, June and October 1982, edited by H. Ehringer, G. Hoyaux and P. A. Pilavachi (Reidel, Dordrecht, 1983) p. 156.
3. *Idem*, in Proceedings of International Seminar on Energy Conservation in Industry, Düsseldorf, February 1984 (VDI, Düsseldorf, 1984) p. 280.
4. C. B. PONTON, R. D. RAWLINGS and P. S. ROGERS, *Proc. Br. Ceram. Soc.* **37** (1986) 229.
5. F. FÖRSTER, *Z. Metallkde* **29** (1937) 109.
6. J. L. LYTTON, J. A. HREN, K. T. KAMBER and O. D. SHERBY, *Br. J. Appl. Phys.* **15** (1964) 1573.
7. S. SPINNER and W. E. TEFFT, *ASTM Proc.* **61** (1961) 1221.
8. ANSI/ASTM C623-71 (Philadelphia) (reapproved 1977), "Standard Test Method for Young's Modulus, Shear Modulus, and Poisson's Ratio for Glass and Glass–Ceramics by Resonance".
9. S. SPINNER and R. C. VALORE Jr, *J. Res. Nat. Bur. Stand.* **60** (1958) 459.
10. G. PICKETT, *ASTM Proc.* **45** (1945) 846.
11. C. ZENER, "Elasticity and Anelasticity of Metals" (University of Chicago Press, 1948) p. 60.
12. H. KOLSKY, "Stress Waves in Solids" (Dover, New York, 1963) p. 103.
13. G. URBAIN, F. CAMBIER, M. DELETTER and M. R. ANSEAU, *Trans. J. Br. Ceram. Soc.* **80** (1981) 139.
14. P. W. McMILLAN, "Glass–Ceramics" (Academic, London, 1979) p. 25.
15. E. SCHREIBER, O. L. ANDERSON and NAOHIRO SOGA, "Elastic Constants and Their Measurement" (McGraw-Hill, New York, 1973) p. 6.
16. J. B. WACHTMAN Jr and W. E. TEFFT, *Rev. Sci. Instr.* **29** (1958) 517.
17. S. SPINNER, *J. Amer. Ceram. Soc.* **39** (1956) 113.
18. W. A. DEER, R. A. HOWIE and J. ZUSSMAN, "An Introduction to the Rock-Forming Minerals" (Longman, London, 1966) p. 99.
19. R. J. KIRKPATRICK, *Amer. Min.* **60** (1975) 798.
20. R. M. WESTON and P. S. ROGERS, *Min. Mag.* **42** (1978) 325.
21. C. H. DONALDSON, T. M. USSELMAN, R. J. WILLIAMS and G. E. LOFGREN, in Proceedings of 6th Lunar Science Conference, Houston, Texas (Pergamon, Oxford, 1975) p. 843.
22. J. B. WACHTMAN Jr and D. G. LAM Jr, *J. Amer. Ceram. Soc.* **42** (1959) 254.
23. M. O. MARLOWE and D. R. WILDER, *ibid.* **48** (1965) 227.
24. MASAHIKO SHIMADA, KEN'ICHI MATSUSHITA, SHUSEI KURATANI, TAIRA OKAMOTO, MITSUE KOIZUMI, KOJI TSUKUMA and TAKAAKI TSUKIDATE, *Commun. Amer. Ceram. Soc.* **67** (1984) C23.
25. R. MORRELL, "Handbook of Properties of Technical and Engineering Ceramics – Part 1: An Introduction for the Engineer and Designer" (HMSO, London, 1985) p. 96.

*Received 12 August*
*and accepted 1 December 1987*